Optik - International Journal for Light and Electron Optics 311 (2024) 171900

Contents lists available at ScienceDirect

Optik - International Journal for Light and Electron Optics

journal homepage: www.elsevier.com/locate/ijleo

Original research article

# Validity of Thin Element Approximation in diffractometry of opaque thick objects

Luis Miguel Sanchez-Brea [a,*], Angela Soria-Garcia [a], Joaquin Andres-Porras [a], Jesus del Hoyo [a], Francisco Jose Torcal-Milla [a,b], Mahmoud Hamdy Elshorbagy [c,d], Veronica Pastor-Villarrubia [c], Javier Alda [c]

[a] Universidad Complutense de Madrid, Applied Optics Complutense Group, Optics Department, Facultad de Ciencias Fisicas, Plaza de las Ciencias, 1, 28040, Madrid, Spain

[b] Departamento de Física Aplicada, Instituto de Investigación en Ingeniería de Aragón (i3a), Grupo de Tecnología Óptica Láser, Universidad de Zaragoza, C/ Pedro Cerbuna 12, 50009, Zaragoza, Spain

[c] Applied Optics Complutense Group, Optics Department, Universidad Complutense de Madrid, Facultad de Óptica y Optometría, C/ Arcos de Jalón, 118, 28037, Madrid, Spain

[d] Faculty of Science, Minia University, 61519 El-Minya, Egypt

ARTICLE INFO

*Keywords:*
Diffraction
Diffractometry
Thin Element Approximation
Size measurement
Wave Propagation Method

ABSTRACT

The Thin Element Approximation (TEA) is widely used in diffraction analyses since it can be applied in efficient plane-to-plane propagation algorithms. While refinements have been developed for dielectric objects to obtain more accurate results, TEA is assumed precise for opaque objects. However, through numerical simulations presented in this work, based on Wave Propagation Method, we analyze the tendency of TEA to overestimate the dimensions of opaque objects in diffractometry. This effect was acknowledged in the case of cylinders, and we obtain similar results for the case of rectangular thick strips. On the other hand, TEA demonstrates a high level of accuracy when applied to objects with thickness concentrated at the center and thin edges, such as the isosceles triangular obstacle. Finally, we analyze objects whose shape is defined using the superellipse function, which is chosen for its versatility in generating objects of equivalent width and maximum thickness but with different shapes just changing a single parameter. Our results highlight the importance of considering the object geometry when employing this approximation in diffraction studies of opaque three-dimensional objects.

## 1. Introduction

The precise determination of the far-field diffraction pattern of three-dimensional (3D) objects holds significance at applications of Optics and Engineering, such as diffractometry, non-destructive testing, and scattering by small particles [1]. Rigorous solutions derived from Maxwell's equations are feasible only for a limited set of special cases, such as spheres, cylinders, half planes, or wedges. For irregular shapes or non-plane incident light beams, heuristic models [2–4] or rigorous numerical simulations [5,6] become necessary to achieve accurate results. However, the viability of numerical approaches is constrained by the processing time and data size, rendering it suitable primarily for analyses of very small objects.

For a fast computation of the far field diffraction pattern, the Fraunhofer approximation is commonly used since it adopts a plane-to-plane scheme [7–9]. Let us consider $u_0(x, y)$ as the incident light field. The Thin Element Approximation (TEA) is used to

* Corresponding author.
*E-mail address:* optbrea@ucm.es (L.M. Sanchez-Brea).

https://doi.org/10.1016/j.ijleo.2024.171900
Received 21 December 2023; Received in revised form 28 May 2024; Accepted 28 May 2024
Available online 30 May 2024

determine the field immediately after the object as

$$u_1(x,y) = t(x,y)u_0(x,y), \tag{1}$$

where the light-matter interaction is condensed in the transmittance function $t(x,y)$. For the case of opaque objects, this transmittance function is simplified to

$$t(x,y) = \begin{cases} 0 & \text{light is absorbed/reflected,} \\ 1 & \text{light is transmitted.} \end{cases} \tag{2}$$

That is, $t(x,y)$ can be obtained as a projection in just a plane. For transparent dielectric objects, the transmittance is determined through an integration between two parallel planes, separated a distance $L$,

$$t(x,y) = e^{ik\int_0^L n(x,y,z)dz}, \tag{3}$$

where $n(x,y,z)$ is the refraction index of the object, $k = 2\pi/\lambda$ is the wavenumber of the incident field, and $L$ is considered very thin so that light entering at coordinate $(x,y)$ on the first face exits at approximately the same coordinate on the second face. When the object presents a uniform refractive index $n$, Eq. (3) results in

$$t(x,y) = e^{ik(n-1)h(x,y)+ikL}, \tag{4}$$

where $h(x,y) = h_2(x,y) - h_1(x,y)$ is the thickness of the object, being $h_1(x,y)$ and $h_2(x,y)$ the topography of the two faces [10].

With this approximation, the three-dimensionality of the object is lost and, although TEA has been extensively used, it does not always provide accurate results for dielectric objects [11,12]. Consequently, refinements have been introduced to enhance its performance in specific scenarios, such as when the light beam presents an oblique incidence [13], when the object induces shadowing in the inclined output beam [14], or when interactions between two surfaces is considered [15].

On the other hand, TEA has been found accurate in the context of diffractometry, that is, the measurement of size of objects using the far field diffraction pattern. The size is determined from the angular separation of two consecutive diffraction minima, $\theta_j$, according to [16]

$$d^j_{TEA} = \frac{\lambda}{\Delta\theta_j}, \tag{5}$$

where $\Delta\theta_j = \theta_j - \theta_{j-1}$. Taking into account the assumption of paraxiallity, the angular separation of diffraction minima remains constant, leading to $d^j_{TEA} = d_{TEA}$, $\forall j$.

Nevertheless, when precise measurements are required, this approximation needs to be revised, since it was demonstrated that it does not always yield accurate results. For instance, in the case of cylindrical objects, Martinez-Anton et al. [17] experimentally showed that the diffraction minima generated by metallic cylindrical wires are not exactly located at the angles predicted by TEA, but the angular distance is smaller. Consequently, an overestimation of the cylinder diameter occurs when Eq. (5) is employed. In response to this discrepancy, heuristic models incorporating optical paths were developed to reconcile the experimental data [18]. From a theoretical point of view, the diameter of thick wires was determined from the rigorous electromagnetic model resulting in [19]

$$d^j_{EM} \approx \frac{\lambda}{\Delta\theta_j} - \delta_1^{p,s}, \tag{6}$$

where $\delta_1^{p,s} = \alpha^{p,s}\lambda^{2/3}d_0^{1/3}$, and $\alpha^p = 0.2163$ and $\alpha^s = 0.0942$ are parameters dependent on the polarization of the incident wave, p and s respectively. This polarization dependence was also found in Ref. [20] using boundary diffraction wave method. This shows that, for a precise determination of the far field diffraction pattern, the three-dimensionality of objects must be considered. Since the analytical determination of the near field interaction is not generally feasible for an object characterized by a refractive index $n(x,y,z)$, except in a few specific cases, numerical analysis needs to be employed. Given the scale of micro-optical objects, $d_0/\lambda \gg 1$, rigorous algorithms such as the Finite Element Method (FEM) or Finite-Difference-Time-Domain (FDTD) become impractical due to extensive computing time and memory storage requirements. In this study, we utilize the Wave Propagation Method (WPM) to determine how the incident light beam interacts with the object and compute the light distribution at the near field. [21–23]. WPM is a fast and accurate algorithm, which facilitates realistic wave-optical simulations beyond the constraints of the Thin Element Approximation for micro-optical components. The method has been contrasted with FEM (Comsol) [22]. After the near field interaction, light propagates at vacuum, and the far field diffraction pattern is computed using the Fast Fourier Transform of a field at a plane after the 3D object.

Initially, we analyze a metallic cylinder to compare the WPM results with those obtained through a rigorous method [19]. The overestimation predicted by TEA is confirmed using WPM, despite the latter being a scalar approach. Subsequently, we examine other 3D opaque objects, such as the rectangular thick strip and the isosceles triangular obstacle. The locations of diffraction minima are determined and contrasted with TEA. The overestimation of width is observed for the thick strip, whereas the triangular obstacle does not exhibit this discrepancy. This observation leads us to propose that TEA is valid when the object is thick at the center but not at the edges. To corroborate this hypothesis, we analyze objects defined by a superellipse [24,25]. By modulating a single parameter, we can transform the shape of the object from a isosceles triangular obstacle to a sphere and a rectangular thick strip. This analysis allows us to identify which shapes permit the use of TEA in diffractometry.

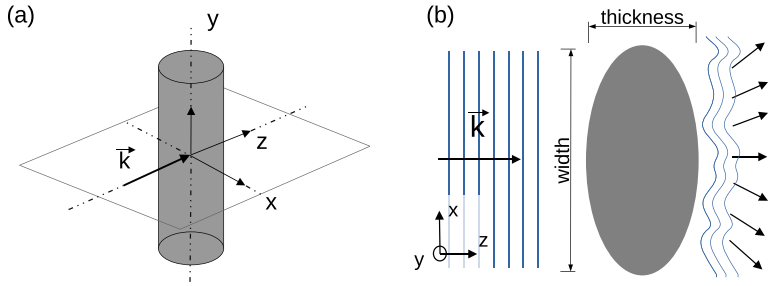


**Fig. 1.** Scheme describing the interaction between an incident plane wave and an infinitely long opaque object. (a) 3D coordinate system. $\vec{k}$ represents a plane wave with wavenumber $k = 2\pi/\lambda$, propagating at z. (b) 2D projection in the XZ plane.

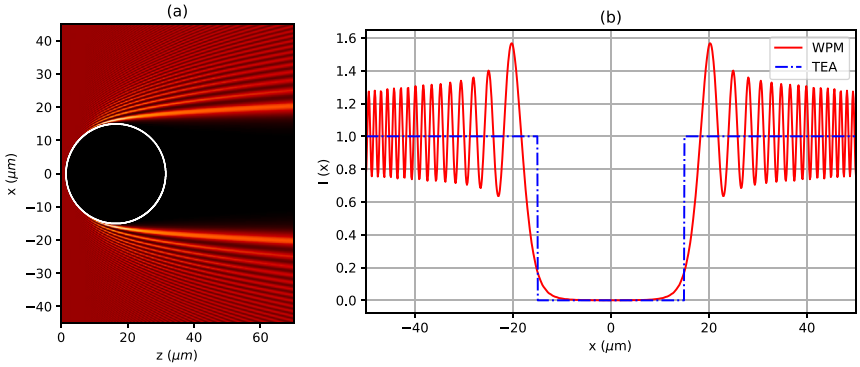


**Fig. 2.** (a) Near-field intensity distribution $I(x, z)$ obtained with WPM algorithm for the case of a steel cylinder with diameter $d_0 = 30$ μm. (b) Diffraction pattern at $z = 70$ μm obtained with WPM (continuous red line), and comparison with the projection of the cylinder proposed by TEA (dash-dotted blue line). (For interpretation of the references to color in this figure legend, the reader is referred to the web version of this article.)

## 2. Far field diffraction pattern produced by opaque objects

For the simulations, let us consider the scheme shown at Fig. 1. A plane wave propagating at $z$-axis, whose wavelength is $\lambda$, illuminates an opaque 3D object, infinitely long, extruded along the $y$-axis. The object is characterized by its complex refractive index $n_c(x, z) = n(x, z) + i\kappa(x, z)$. The refractive index has no dependence with $y$ as the cross section XZ keeps unchanged along the $y$-axis. Therefore, the problem is reduced to 2D in the XZ plane. The width of the opaque object is the size of its projection in the XY plane and the thickness is the size of its projection in the YZ plane. Without loss of generality, we have considered that the incident field, $u_0(x)$, is a plane wave in normal incidence with a wavelength of $\lambda = 0.6328$ μm. The objects are made of stainless steel, whose refractive index is determined experimentally, $n_c = 2.33 + 3.30i$ for this wavelength.

The procedure for determining the location of diffraction minima is outlined as follows: in the first place we compute the near-field interaction between the light beam and the object using the open-source package Diffraction [26,27]. The simulations are performed in 2D, in the XZ plane, which allows a significant reduction in computational time. A high sampling rate $65,000 \times 12,000$ pixels in the x-z plane is employed to avoid numerical artifacts that might affect the location of diffraction minima. The simulation result of the near-field interaction is $u_{WPM}(x, z)$. The propagation is carried out up to a distance $z$ far enough from the object, at least $20\lambda$. We extract the field at the last plane of the simulation, $u_1(x) = u_{WPM}(x, z_{\max})$, and the Fast Fourier Transform algorithm (FFT) is applied to $u_1(x)$ in order to determine the far-field diffraction pattern, $\widetilde{u}(\theta)$. Finally, the angular locations of the diffraction minima, $\theta_j$, are obtained. The object's width is estimated using Eq. (5). For comparison, we also determine the width using TEA. In this case, it is assumed that the incident field is masked by a thin strip, whose width is equal to the projection in the $z$-axis.

### 2.1. Metallic cylinder

Our first numerical analysis is devoted to the cylinder for comparison with the analytical model. For the case of the cylinder, it is possible to obtain a rigorous solution from the classical Mie scattering theory [1,28,29] as a series expansion form that converges sufficiently quickly when the radius is much smaller than the wavelength. In addition, a transformation allows to derive an asymptotic expansion for cylinders with a radius much larger than the wavelength of the incident beam [30]. Using this rigorous solution, Sanchez-Brea predicted a systematic overestimation when using the Fraunhofer diffraction formula to determine the cylinder diameter [19]. Recently, precise alternative expressions for determining the intensity the distribution diffracted by an infinitely long circular cylinder normally illuminated by a plane wave have been obtained [31].

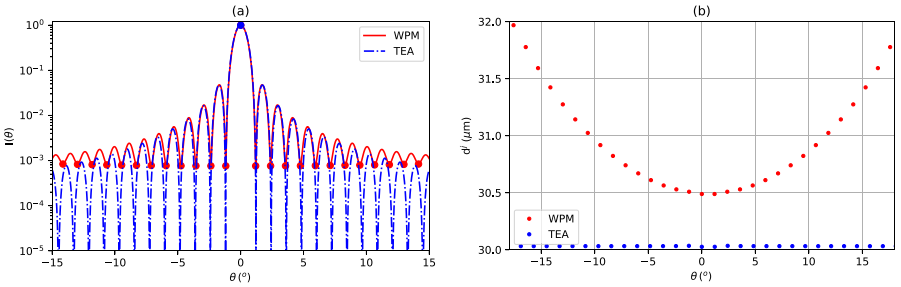


**Fig. 3.** Diameter estimation for the field distribution at Fig. 2. (a) Far field diffraction pattern for thick cylinder and TEA. Dots are the location of the diffraction minima. (b) Diameters estimated using Eq. (5).

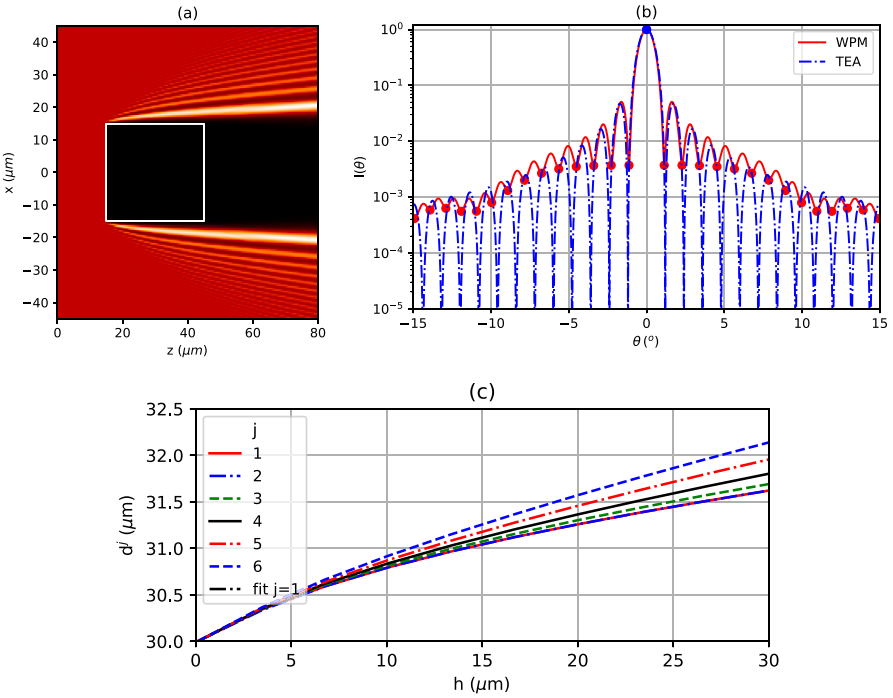


**Fig. 4.** (a) Intensity distribution using WPM for a rectangular thick strip with a width $d_0 = 30$ μm and thickness $h = 30$ μm, (b) Far field diffraction pattern with WPM and with TEA. The difference between both diffraction patterns is clear. (c) Width estimation $d^j$, for strips with $d_0 = 30$ μm and different values of thickness. This estimation is performed for diffraction orders $j = 1, \ldots, 6$. Also, the fitting to order $j = 1$ is shown.

For the numerical results, Fig. 2a depicts the field $u_{WPM}(x, z)$ generated by the interaction of the plane wave with a cylinder whose diameter is $d_0 = 30$ μm. The intensity distribution after the cylinder exhibits discernible ripples, which have been explained considering the interference between the incident and reflected fields [18]. Using the last plane computed in the simulation $u_1(x, y)$, Fig. 2b, we calculate the intensity distribution at the far field employing the Fraunhofer approach, as illustrated in Fig. 3a. The locations of the diffraction minima obtained through the WPM approach do not coincide with those predicted by TEA. By comparing the differences in diameter estimation for both diffraction patterns using Eq. (5), the overestimation of WPM is clear, as depicted in Fig. 3b.

Furthermore, we can see that the diameter estimation increases quadratically with the diffraction order $j$, which is not predicted in [19] due to simplifications of the equations. The lowest value occurs for $j = 1$, being $\Delta d = 0.497$ μm. This value coincides well with the prediction by Eq. (6) for p-polarization, $\Delta d^p = 0.495$ μm, despite the scalar nature of WPM in handling diffraction.

### 2.2. Rectangular thick strip

The analysis of the metallic cylinder has confirmed the validity of the numerical procedure employed for determining the location of diffraction minima and, consequently, the diameter of the obstacle. Now, we turn our attention to the case of a rectangular thick strip. Fig. 4a illustrates the near-field intensity distribution for a steel strip with a width $d_0 = 30$ μm and a thickness $h = 30$ μm. In

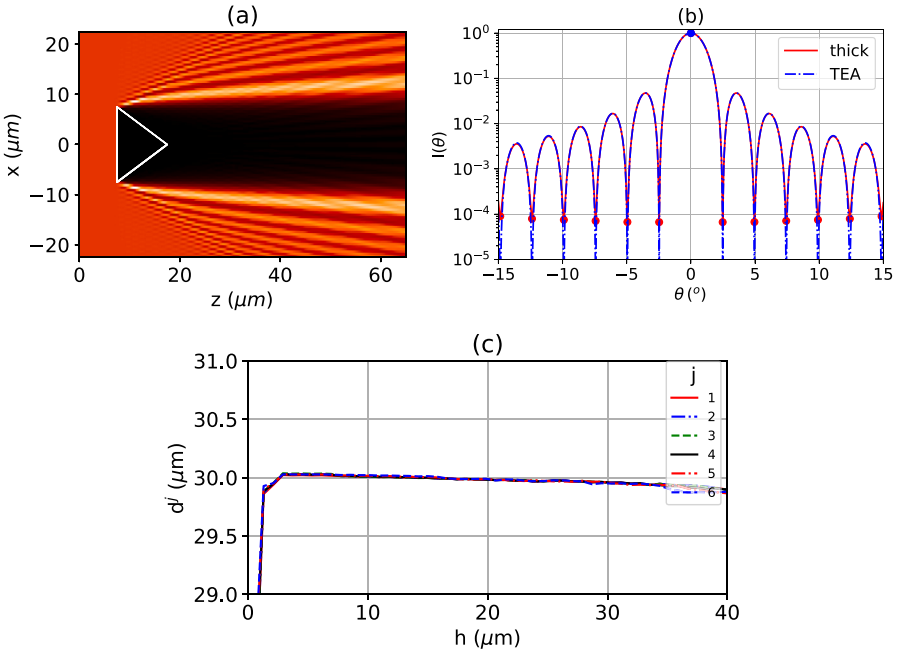


**Fig. 5.** (a) Intensity distribution using WPM for a isosceles triangular obstacle with a width $d_0 = 30$ μm and thickness $h = 10$ μm. (b) Far field diffraction pattern computed with WPM and with TEA. We can see that both diffraction patterns coincide. (c) Width estimation $d^j$, for isosceles triangular obstacles with a width $d_0 = 30$ μm and different values of thickness. This estimation is performed for diffraction orders $j = 1, \dots, 6$.

this instance, the overestimation is approximately $\Delta d^1 = d^1 - d_0 \approx 1.47$ μm, where $d^j$ represents the width estimation for order $j$, a value considerably larger than the predicted for the cylinder with the same width.

Next, we explore the effect of the strip thickness on the width estimation. For this purpose, we compute the width for different strips, with a width $d_0 = 30$ μm, but varying in thickness $h$. The results are presented in Fig. 4c. It is clear that when the strip is very thin, TEA is valid and the diameter is $d^j \approx d_0$ for all diffraction orders. However, as the thickness increases, an overestimation of the strip width emerges, and this overestimation is dependent on the considered diffraction order. Specifically, for order $j = 1$, the relative error $\sigma_j = \left(d^j - d_0\right)/d_0$ can be as high as 5% for a thickness $h = 30$ μm (square). For this case, we have fitted the dependence of $d^1$ with the thickness of the obstacle resulting in $d^1 = 29.94 + 0.1968\, h^{0.634}$ μm. The slope is similar to the value $\alpha^p = 0.2163$.

### 2.3. Isosceles triangular obstacle

In previous sections, an overestimation of the width is observed when TEA is applied to diffractometry of thick objects. This prompts further consideration of the origin of the overestimation. To explore this, let us examine an absorbent isosceles triangular obstacle, that is very thin at the edges and thicker at the center. Fig. 5a depicts the near-field intensity distribution around an isosceles triangular obstacle with a width $d_0 = 30$ μm and maximum thickness $h = 10$ μm. Additionally, the far-field diffraction pattern for this simulation is presented in Fig. 5b. Remarkably, even though the object is thick, the far-field diffraction pattern coincides with that predicted by TEA.

Next, we investigate the effects of increasing the thickness of the triangular obstacle. Fig. 5c illustrates the size estimation using the WPM algorithm for various thickness values. When the triangular obstacle is very thin, there is a subestimation of the triangular obstacle size, as the finite attenuation index of the material allows light to pass through the edges. For thickness values in the range $d_0 \in (3\,\mu\text{m}, 40\,\mu\text{m})$, the results obtained with WPM and TEA coincide significantly. For this range, the relative error $\sigma_j$ is lower than 0.3% for the orders 1-6. There is a slight decrease in the estimated width of the triangle as its thickness increases. We believe this is due to the portion of the diffracted light that reaches the lateral surfaces of the object and is reflected. This reflected light changes direction upon reflection, interferes with the light diffracted by the edge, and slightly alters the position of the diffraction minima.

## 3. Variation in shape of the thick object

Now let us generalize the analysis for 3D obstacles with the same width and thickness but a different shape. For this purpose, we will employ the superellipse function, defined as

$$\left|\frac{x-x_0}{r}\right|^\gamma + \left|\frac{z-z_0}{h}\right|^\gamma = 1 \qquad \forall z \geq z_0, \tag{7}$$

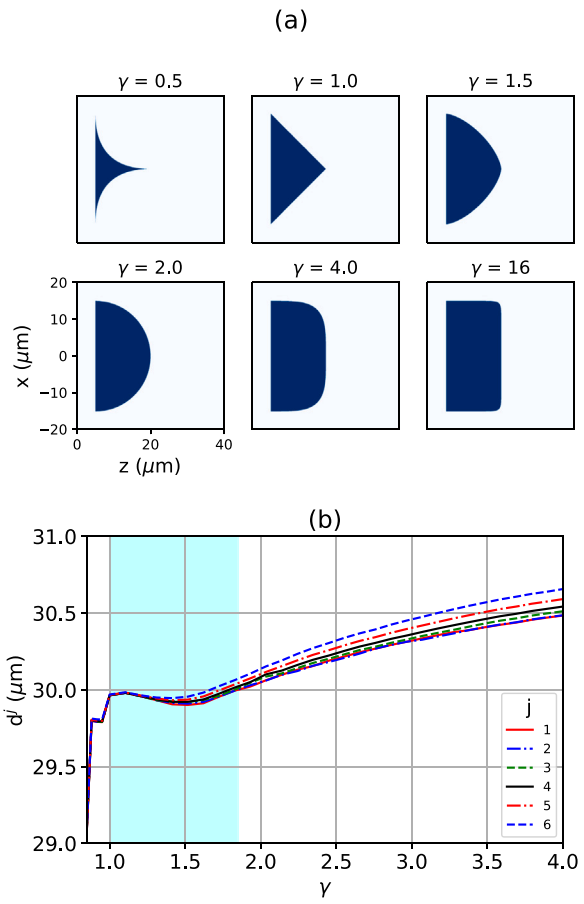


**Fig. 6.** (a) Superellipses used in the simulations, with different values of shape parameter $\gamma$, width $d_0 = 30$ μm, and thickness $h = 15$ μm. (b) Estimated width using WPM for superellipses with different shape parameter, $\gamma$. The blue area $\gamma \in (1, 1.85)$ represents the shapes where TEA is approximately valid, between the two positions where the estimated diameter using WPM is $d^1 = d_0$. (For interpretation of the references to color in this figure legend, the reader is referred to the web version of this article.)

where we have truncated the definition to positions $z \geq z_0$, $(x_0, z_0)$ is the position of the left-center of the obstacle, $d_0 = 2r$ is its width, $h$ is its thickness, and $\gamma$ is the shape factor. This definition includes the following cases: isosceles triangular obstacle, $\gamma = 1$; semi-cylinder, $\gamma = 2$ and $r = h$; and thick strip, $\gamma = \infty$. Some example of superellipses are shown in Fig. 6a.

The width estimation for superellipses with a width $d_0 = 30$ μm, and thickness $h = 15$ μm is depicted in Fig. 6b as a function of the shape parameter $\gamma$. Initially, for values of $\gamma < 1$, the edges are so thin, that light is able to pass through the object, resulting in a width estimation lower than $d_0$. Subsequently, there exists a range of the $\gamma$ parameter where $d^j \approx d_0$, indicating the validity of TEA. For this specific case, the range corresponds approximately to $\gamma \in (1, 1.85)$. Beyond this range, for greater values of $\gamma$, an overestimation occurs, and TEA is not longer valid.

## 4. Conclusions

In summary, we have analyzed the validity of the Thin Element Approximation (TEA) for far-field diffractometry of opaque thick objects, infinitely long, extruded along the y-axis. The Wave Propagation Method was employed as a more rigorous numerical algorithm to determine the near field interaction between the incident field and the three-dimensional object. After, the far field was computed using the Fast Fourier Transform, and the location of the diffraction minima was compared to that predicted by TEA. The overestimation of TEA was observed for the cylinder, consistent with previous analytical results. This overestimation depends on the diffraction order, being lower for the lowest orders. A subsequent analysis of the rectangular thick strip revealed similar results. However, no overestimation was observed for the isosceles triangular obstacle, due to its very thin edges. Finally, the far field diffraction pattern produced by an object defined with the superellipse function was computed. This function allows to generate objects with the same width and thickness but different shapes by modifying just one parameter $\gamma$. TEA was found to be invalid for $\gamma < 1$, resulting in a subestimation of the width as the optical field penetrated through the object. For the studied cases, TEA is a good approximation for determining width of the object in the range $\gamma \in (1, 1.85)$. However, for greater values of $\gamma$, a significant overestimation of the width was observed.

## CRediT authorship contribution statement

**Luis Miguel Sanchez-Brea:** Writing – original draft, Supervision, Software, Methodology, Funding acquisition, Data curation, Conceptualization. **Angela Soria-Garcia:** Writing – review & editing, Software. **Joaquin Andres-Porras:** Software, Formal analysis. **Jesus del Hoyo:** Writing – review & editing, Software. **Francisco Jose Torcal-Milla:** Writing – review & editing, Validation, Software. **Mahmoud Hamdy Elshorbagy:** Writing – review & editing, Software. **Veronica Pastor-Villarrubia:** Writing – review & editing, Software. **Javier Alda:** Writing – review & editing, Funding acquisition, Formal analysis.

## Declaration of competing interest

The authors declare that they have no known competing financial interests or personal relationships that could have appeared to influence the work reported in this paper.

## Data availability

Data will be made available on request.

## Acknowledgments

The authors acknowledge funding support from the "Nanorooms" PID2019-105918GB-I00 project (Proyectos de Generación de Conocimiento 2019) and the "VDOEST "PID2022-138071OB-I00 project (Proyectos de Generación de Conocimiento 2022) from the Ministerio de Ciencia e Innovación of Spain MCIN/AEI/10.13039/501100011033/FEDER, EU.

## References

[1] C.F. Bohren, D.R. Huffman, Absorption and Scattering of Light by Small Particles, John Wiley & Sons, 2008.
[2] J.B. Keller, Geometrical theory of diffraction, J. Opt. Soc. Am. 52 (2) (1962) 116–130.
[3] G.L. James, Geometrical Theory of Diffraction for Electromagnetic Waves, (no. 1) IET, 1986.
[4] V.A. Borovikov, V.A. Borovikov, B.Y. Kinber, B.E. Kinber, Geometrical Theory of Diffraction, (no. 37) Iet, 1994.
[5] D.M. Sullivan, Electromagnetic Simulation Using the FDTD Method, John Wiley & Sons, 2013.
[6] M.N.O. Sadiku, Computational Electromagnetics with Matlab, CRC Press, 2018.
[7] W. Tang, Y. Zhou, J. Zhang, Improvement on theoretical model for thin-wire and slot measurement by optical diffraction, Meas. Sci. Technol. 10 (11) (1999) 119–123, http://dx.doi.org/10.1088/0957-0233/10/11/401.
[8] S.A. Khodier, Measurement of wire diameter by optical diffraction, Opt. Laser Technol. 36 (1) (2004) 63–67, http://dx.doi.org/10.1016/S0030-3992(03)00134-8.
[9] Salvatore Ganci, Fraunhofer diffraction by a thin wire and Babinet's principle, Am. J. Phys. 73 (1) (2005) 83–84, http://dx.doi.org/10.1119/1.1791274.
[10] J.W. Goodman, Introduction to Fourier Optics, Roberts and Company publishers, 2005.
[11] D.A. Pommet, M.G. Moharam, E.B. Grann, Limits of scalar diffraction theory for diffractive phase elements, J. Opt. Soc. Amer. A 11 (6) (1994) 1827, http://dx.doi.org/10.1364/josaa.11.001827.
[12] T. Vallius, P. Vahimaa, M. Honkanen, Electromagnetic approach to the thin element approximation, J. Modern Opt. 51 (14) (2004) 2079–2092, http://dx.doi.org/10.1080/09500340412331286612.
[13] M. Testorf, Perturbation theory as a unified approach to describe diffractive optical elements, J. Opt. Soc. Amer. A 16 (5) (1999) 1115, http://dx.doi.org/10.1364/josaa.16.001115.
[14] U. Levy, E. Marom, D. Mendlovic, Thin element approximation for the analysis of blazed gratings: Simplified model and validity limits, Opt. Commun. 229 (1–6) (2004) 11–21, http://dx.doi.org/10.1016/j.optcom.2003.10.017.
[15] C. Neipp, J.T. Sheridan, A. Márquez, S. Gallego, M. Ortuño, A. Beléndez, I. Pascual, Effect of the glass substrate on the efficiency of the different orders that propagate in a transmission sinusoidal diffraction grating, J. Modern Opt. 53 (10) (2006) 1403–1410, http://dx.doi.org/10.1080/09500340600551895.
[16] M. Born, E. Wolf, Principles of Optics: Electromagnetic Theory of Propagation, Interference and Diffraction of Light, Elsevier, 2013.
[17] J.C. Martínez-Antón, I. Serroukh, E. Bernabeu, On Babinet's principle and a diffraction-interferometric technique to determine the diameter of cylindrical wires, Metrologia 38 (2) (2001) 125–134, http://dx.doi.org/10.1088/0026-1394/38/2/4.
[18] E. Bernabeu, I. Serroukh, L.M. Sanchez-Brea, Geometrical model for wire optical diffraction selected by experimental statistical analysis, Opt. Eng. 38 (8) (1999) 1319, http://dx.doi.org/10.1117/1.602173.
[19] L.M. Sanchez-Brea, Diameter estimation of cylinders by the rigorous diffraction model, J. Opt. Soc. Amer. A 22 (7) (2005) 1402, http://dx.doi.org/10.1364/josaa.22.001402.
[20] J. Xie, Y. Qiu, H. Ming, C. Li, Light polarization effect in measurement of thin wire diameter by laser diffraction and its explanation with boundary diffraction wave, J. Appl. Phys. 69 (10) (1991) 6899–6903, http://dx.doi.org/10.1063/1.347679.
[21] K.H. Brenner, W. Singer, Light propagation through microlenses: a new simulation method, Appl. Opt. 32 (26) (1993) 4984–4988, http://dx.doi.org/10.1364/ao.32.004984.
[22] S. Schmidt, T. Tiess, S. Schröter, R. Hambach, M. Jäger, H. Bartelt, A. Tünnermann, H. Gross, Wave-optical modeling beyond the thin-element-approximation, Opt. Express 24 (26) (2016) 30188, http://dx.doi.org/10.1364/oe.24.030188.
[23] K.H. Brenner, A high-speed version of the wave propagation method applied to micro-optics, in: 2017 16th Workshop on Information Optics, WIO 2017, (no. 1) 2017, pp. 2–4, http://dx.doi.org/10.1109/WIO.2017.8038108.
[24] J. Gielis, A generic geometric transformation that unifies a wide range of natural and abstract shapes, Am. J. Bot. 90 (3) (2003) 333–338, http://dx.doi.org/10.3732/ajb.90.3.333.
[25] Wikipedia, Superellipse, https://en.wikipedia.org/wiki/Superellipse.
[26] L.M. Sanchez-Brea, Diffractio - pypi, 2019, https://pypi.org/project/diffractio/.
[27] L.M. Sanchez-Brea, Diffractio - Readthedocs, 2019, https://diffractio.readthedocs.io/en/latest/.
[28] G. Mie, Beiträge zur Optik trüber Medien, speziell kolloidaler Metallösungen, Ann. Phys. 330 (3) (1908) 377–445.
[29] P. Debye, Das elektromagnetische Feld um einen Zylinder und die Theorie des Regenbogens, Phys. Z 9 (1464) (1908) 775–778.
[30] Hönl H., Maue A.W., Westpfahl K., Handbuch der Physik, vol. XXV, J. Springer, 1961, pp. 495–531.
[31] J. Shen, X. Jia, Diffraction of a plane wave by an infinitely long circular cylinder or a sphere: Solution from Mie theory, Appl. Opt. 52 (23) (2013) 5707–5712, http://dx.doi.org/10.1364/AO.52.005707.